Volume 4
Number 5
7 March 2022
Pages 1237–1484

Nanoscale Advances

rsc.li/nanoscale-advances

ISSN 2516-0230

ROYAL SOCIETY OF CHEMISTRY

COMMUNICATION

Ning Wen *et al.*

Graphene-containing metal–organic framework nanocomposites for enhanced microwave ablation of salivary adenoid cystic carcinoma

NCNST

Nanoscale Advances

ROYAL SOCIETY OF CHEMISTRY

COMMUNICATION

View Article Online
View Journal | View Issue

Cite this: *Nanoscale Adv.*, 2022, **4**, 1308

Received 6th October 2021
Accepted 15th January 2022

DOI: 10.1039/d1na00729g

rsc.li/nanoscale-advances

Graphene-containing metal–organic framework nanocomposites for enhanced microwave ablation of salivary adenoid cystic carcinoma†

Ruozhen Li,[ab] Yaping Tian,[c] Biao Zhu,[b] Yu Wang,[d] Ruijie Dang,[b] Lisheng Zhao,[b] Shuo Yang,[b] Yunxia Li[b] and Ning Wen *[b]

Salivary adenoid cystic carcinoma (SACC), one of the most common malignant tumors in the head and neck region, is characterized by high postoperative recurrence rate and poor prognosis. Microwave (MW) ablation possesses advantages in preserving SACC patients' facial aesthetics and oral function, but unfortunately, it suffers from low therapeutic efficacy due to the limited MW-thermal efficiency. Moreover, the insufficient thermal ablation may aggravate hypoxic state in tumors, which is deleterious to the treatment of residual tumors and aggressive tumors. Hence, MW ablation has been rarely applied in treating head and neck tumors in recent years. To minimize the unfavorable outcomes and maximize the therapeutic effects of MW ablation, a MW sensitizer coupled with a self-sufficient oxygen nanoagent was employed for the first time in MW ablation to treat head and neck tumors. We prepared a graphene-containing metal–organic framework (ZIF67@Gr-PEG), which exhibited excellent MW thermal conversion ability endowed by the incorporated Gr and showed *in situ* oxygen generation capacity derived from the ZIF67 matrix. In an animal experiment, ZIF67@Gr-PEG-based MW ablation with a temperature up to 66.1 °C exhibited a high tumor ablation rate. More importantly, insufficient MW ablation-induced high expressions of HIF-1α and VEGF were observed in our experiment, whereas the levels of tumor hypoxia and angiogenesis were efficiently decreased in MW ablation with the assistance of ZIF67@Gr-PEG nanocomposites (NCs). Notably, our strategy for MW ablation not only evidences the great potential of ZIF67@Gr-PEG but also promotes the translation of thermotherapeutic graphene from basic research to clinical practice.

1. Introduction

Salivary adenoid cystic carcinoma (SACC) is a malignant neoplasm that most commonly arises from the salivary glands of the head and neck. It is characterized by slow but relentless and infiltrating growth and hematogenous dissemination.[1] Although SACC tumors are histologically low grade and slow-growing, their distant metastasis rate can be as high as 40%–60%.[2,3] Surgery alone or in combination with postoperative radiotherapy enables effective locoregional control of SACC but fails to block tumor progression and recurrence.[4,5] Chemotherapy has been demonstrated to make only minor contribution to SACC-cancer survival.[6,7] Therefore, current treatments for highly aggressive SACC cancers remain unsatisfactory. In addition, surgery operation for treatment of tumors in the head and neck region is often accompanied by facial injuries, function impairment and mental suffering. MW ablation is minimally invasive, with advantages in preserving SACC patients' facial aesthetics and oral function as well as evoking immune response and other therapeutic responses, but unfortunately, it suffers from low therapeutic efficacy due to the limited MW-thermal efficiency.[8–10] Moreover, insufficient thermal ablation could induce angiogenesis and aggravate hypoxia in tumors, resulting in increased local recurrence and distance metastasis. Accumulating evidence has shown that high expressions of VEGF and CD31 and elevation of HIFs were observed after insufficient MW ablation[11–13] and insufficient radiofrequency ablation (RFA).[14–19] Inhibition of tumor recurrence following MW ablation remains a challenge in clinic, as evidenced by three-year clinical postablation recurrence data,[20] which threatened the prognosis and lifetime of patients with cancer. Hence, MW ablation has been rarely applied in treating head and neck tumors in recent years. To minimize the unfavorable outcomes and maximize the therapeutic effects of MW ablation, a MW sensitizer coupled with an oxygen nanoagent has been applied in MW ablation.[21,22] MW sensitizers can improve the precision and safety of MW ablation by effectively accumulating heat into the whole tumor region.[23–31] Different from most MW sensitizers based on the principle of ions

[a]*Medical School of Chinese PLA, Beijing 100853, China*

[b]*Department of Stomatology, The First Medical Center, Chinese PLA General Hospital, No. 28 Fuxing Road, Beijing 100853, China. E-mail: wenningchn@163.com*

[c]*Birth Defects Prevention and Control Technology Research Center, Translational Medicine Research Center, Chinese PLA General Hospital, 28 FuXing Road, Beijing 100853, China*

[d]*Department of Oncology, Air Force Medical Center, PLA, No. 30 FuCheng Road, Haidian District, Beijing 100142, China*

† Electronic supplementary information (ESI) available. See DOI: 10.1039/d1na00729g

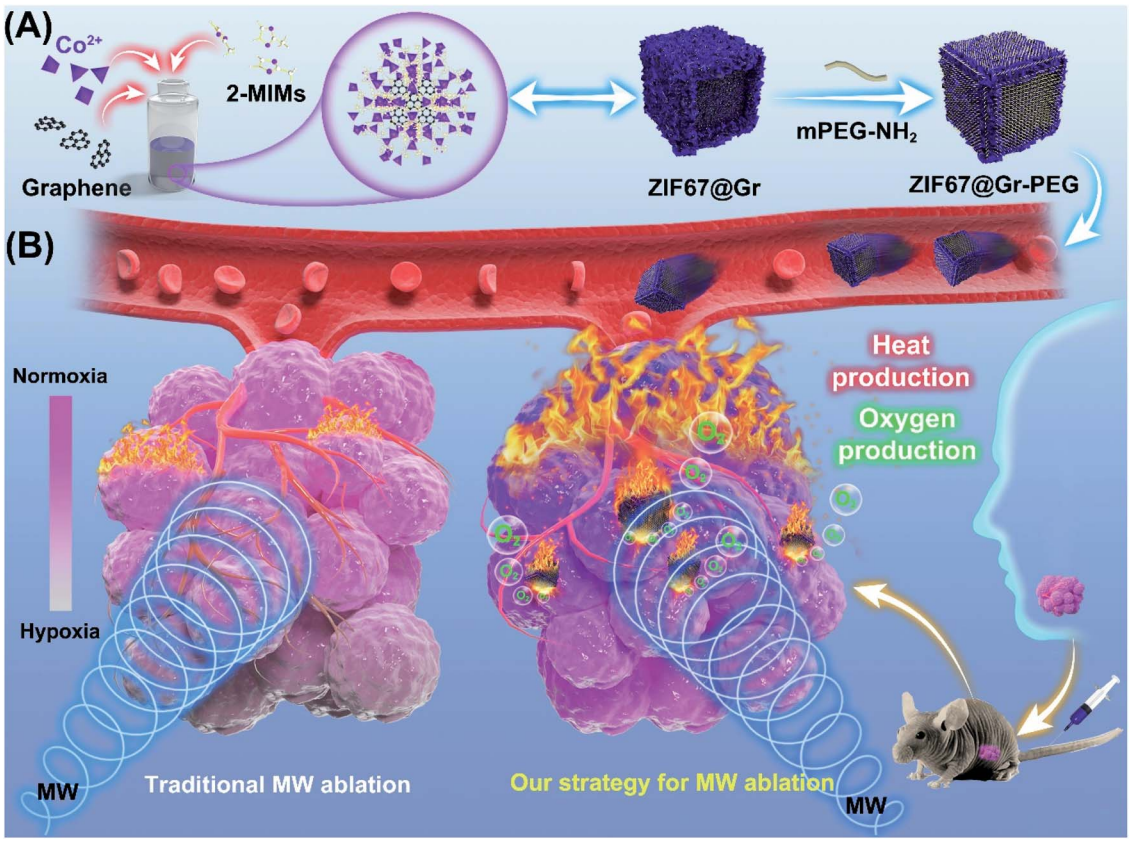

Scheme 1 (A) Preparation procedure of the ZIF67@Gr-PEG nanocomposite. (B) Traditional MW ablation without ZIF67@Gr-PEG NCs may result in insufficient ablation and aggravation of tumor hypoxia. Our strategy for MW ablation with ZIF67@Gr-PEG NCs achieved the combined effects of enhanced MW ablation and tumor hypoxia relief.

vibrating in a confined space,[28–30] graphene (Gr) has excellent thermotherapeutic effects due to its low-frequency microwave absorption properties and good thermal conversion ability.[31,32] Given the high-purity, small-size and microwave responsive characteristics of this biocompatible graphene, its applications in the clinical field have drawn wide attention. Nevertheless, the harsh tumor microenvironment, especially the hypoxia after insufficient ablation, could be a major risk factor affecting the long-term success of graphene-based MW ablation against tumor recurrence and metastasis. It also limits the potential translation of thermotherapeutic graphene into clinic. Consequently, thermo-sensitive graphene coupled with an oxygen self-sufficient nanoplatform is emerging as an efficient anti-tumor nanoagent. Various oxygen-producing nanoagents, such as manganese dioxide, perfluorocarbon, and catalase- or metal-catalyzed endogenous peroxides have been used to relieve tumor hypoxia,[33–35] but all of them lack the unique advantages of metal–organic frameworks (MOFs), including unprecedented larger surface areas, tailorable pore structures, and good thermal stability. Inspired by the efficient catalytic performance of the zeolitic imidazolate framework-67 (ZIF67) for hydrogen peroxide,[36] we designed a multifunctional nanocomposite by coupling ZIF67 with graphene for efficient tumor therapy.

In this work, a graphene-containing metal–organic framework (ZIF67@Gr) was prepared *via* a facile one-pot route at room temperature, by introducing graphene into the zeolitic imidazolate framework-67 (ZIF67) growth medium during the self-assembly process (Scheme 1). Thereafter, ZIF67@Gr was modified with PEG to improve its dispersibility and biocompatibility.[36,37] Herein, the obtained ZIF67@Gr-PEG NCs exhibited excellent MW thermal conversion ability endowed by the incorporated Gr and showed *in situ* oxygen generation capacity derived from the ZIF67 matrix. Additionally, the MW thermal and hypoxia relief effects could combine to trigger intrinsic an immune response.[38,39] ZIF67@Gr-PEG would, therefore, serve as a multi-functional nanoagent for effective anti-tumor application by combing with tumor hypoxia amelioration, high-performance MW ablation and activation of innate immune responses. The effective combination of multiple mechanisms in our strategy is thought to be important for the long-term inhibition of aggressive malignant tumors with a high rate of recurrence and metastasis. Notably, in an animal experiment, high expressions of HIF-1α and VEGF were observed after insufficient MW ablation, while our new strategy for MW ablation could enhance the ablation efficiency and reduce the level of hypoxia in tumors. Thus, ZIF67@Gr-PEG-based MW ablation was applied in head and neck tumors for the first time. This highly efficient and minimally invasive strategy is superior to conventional surgical treatment in that it can preserve aesthetics, function and mental health, the lack of which has long troubled the majority of head

and neck cancer patients. In addition, application of graphene/MOF-based composites, alone, or in combination with other treatments, such as immunotherapy and chemoradiotherapy, promotes the preclinical to clinical translation of thermotherapeutic graphene in MW ablation therapy.

2. Results and discussion

2.1. Synthesis and characterization of ZIF67@Gr-PEG NCs

Transmission electron microscopy (TEM) was firstly employed to determine the morphology and structure of the prepared ZIF67@Gr NCs. TEM images (Fig. 1A and B) revealed that ZIF67@Gr had the same hexahedral structure as pure ZIF67. As shown in Fig. 1C, the average hydrodynamic diameter of ZIF67@Gr NCs was about 334.4 nm. To enhance ambient stability and biocompatibility, mPEG-NH_2 was modified onto the surface of ZIF67@Gr NCs. The zeta potentials of −0.5, 10.6 and 5.0 mV for Gr, ZIF67@Gr and ZIF67@Gr-PEG respectively suggested the successful synthesis of ZIF67@Gr-PEG NCs (Fig. 1D). Surface charge plays an important role in governing the *in vivo* fate of nanoparticles.[40] In our work, positively charged ZIF67@Gr-PEG is favorable for cellular phagocytosis, which helps exert the catalytic activity of our nanocomposites. At the same time, PEG modification would reduce the elimination of ZIF67@Gr-PEG by the immune system during blood circulation.[41] In addition, as shown in Fig. 1E, the UV-vis absorption spectra exhibited the successful embedment of Gr in ZIF67 and loading of PEG on ZIF67@Gr NCs. ZIF67@Gr showed a characteristic absorption peak in accordance with the typical absorption of ZIF67. Furthermore, the crystal structures of synthesized ZIF67@Gr, ZIF67 and Gr were also confirmed by X-ray diffraction (XRD) tests. As shown in Fig. 1F, the similar diffractive pecks observed in XRD of pure ZIF67 and ZIF67@Gr indicated that Gr-doping did not impact the crystalline integrity of ZIF67, which agreed well with the results obtained by TEM. The above characterization confirmed the successful synthesis of ZIF67@Gr-PEG and the following studies were conducted to investigate its physicochemical properties.

2.2. Evaluation of MW heating effects *in vitro*

We explored the *in vitro* MW thermal conversion capability of ZIF67@Gr-PEG NCs using a forward-looking infrared (FLIR) thermal imager. Under 0.9 W MW irradiation (450 MHz) for 5 min, the temperature of a simple saline solution group increased from 26.1 °C to 43 °C (ΔT = 16.9 °C), whereas the temperature of the saline solution of ZIF67@Gr-PEG NCs increased from 26.5 °C to 54.2 °C (ΔT = 27.7 °C) at 4 mg mL^{-1} under the same conditions (Fig. 2B). The large difference of temperature variations (10.8 °C) between the two groups was due to the good MW thermal conversion ability of ZIF67@Gr-PEG NCs. Besides, under MW irradiation (450 MHz), ZIF67@Gr-PEG NCs displayed an apparent concentration-dependent increase in the temperature profile (Fig. 2A and B). After 5 min of irradiation, the final temperature rise (ΔT) of ZIF67@Gr-PEG NC dispersions at different concentrations of 1, 2, and 4 mg mL^{-1} were 5.6, 9 and 10.8 °C higher than that of the NaCl group, respectively (Fig. 2C). The corresponding infrared images are shown in Fig. 2A. MW heating experiment showed that ZIF67@Gr-PEG NCs could act as a MW sensitizer for enhanced MW ablation therapy.

2.3. Evaluation of generation of oxygen *in vitro*

We investigated the *in vitro* oxygen generation ability of ZIF67@Gr-PEG NCs under MW irradiation. The amount of

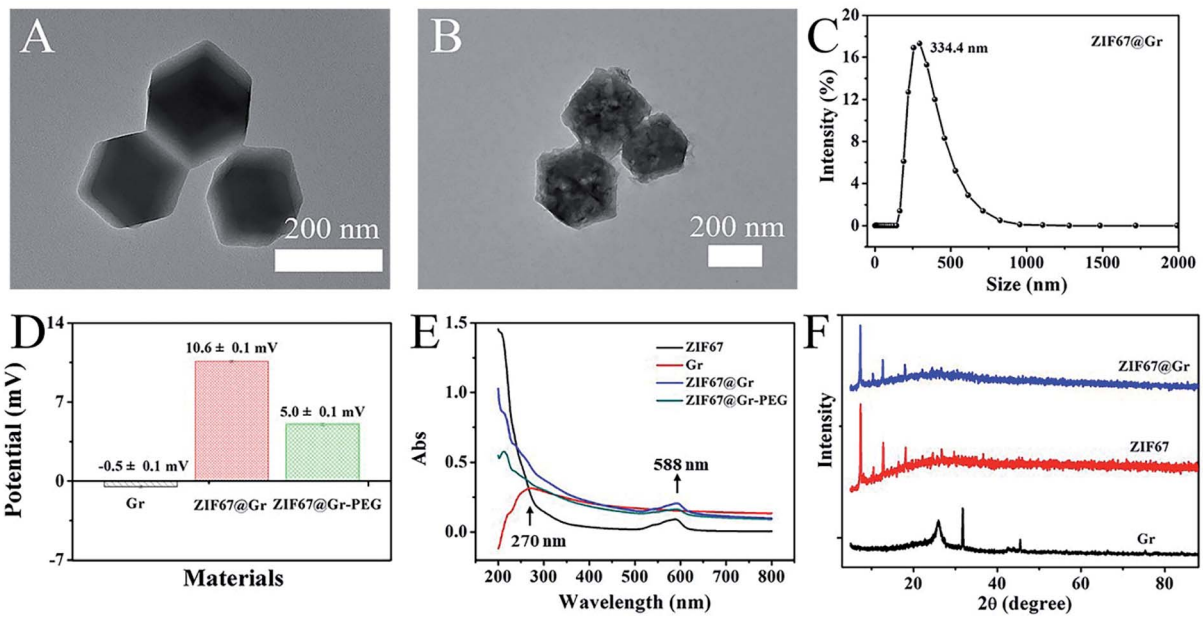

Fig. 1 Characterization of ZIF67@Gr-PEG. TEM images of (A) ZIF67 NCs and (B) ZIF67@Gr NCs. The scale bar is 200 μm. (C) Hydrodynamic diameter of ZIF67@Gr. (D) Zeta potentials of Gr, ZIF67@Gr and ZIF67@Gr-PEG. (E) UV-vis spectra of Gr, ZIF67, ZIF67@Gr and ZIF67@Gr-PEG. (F) XRD patterns of Gr, ZIF67, and ZIF67@Gr.

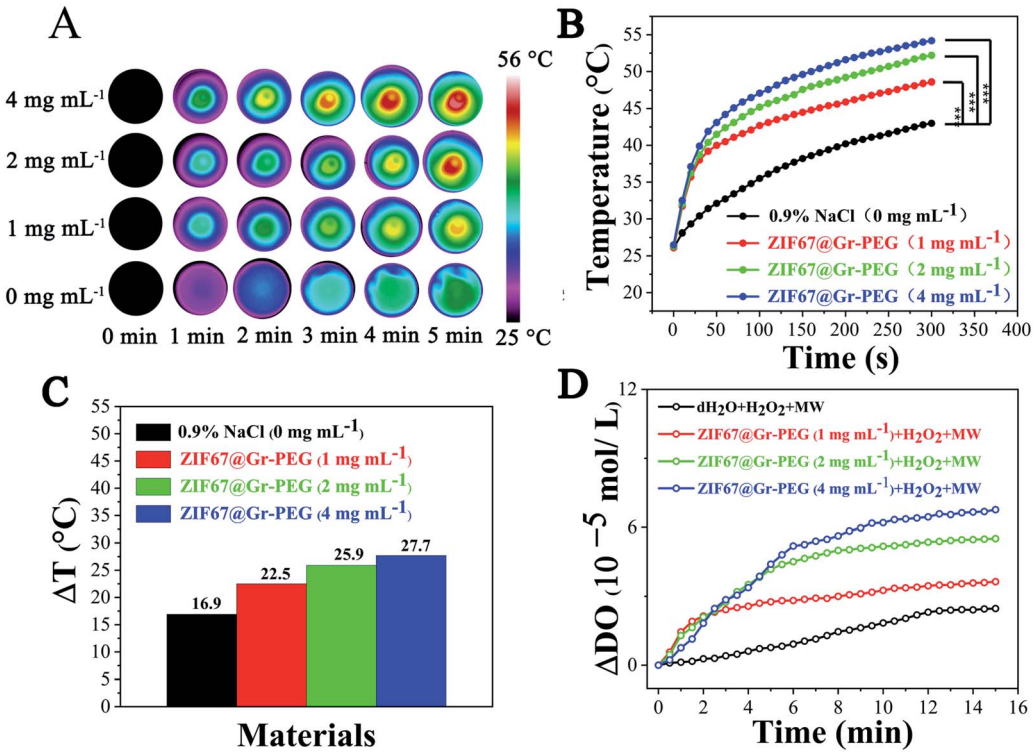

Fig. 2 Functional properties of ZIF67@Gr-PEG NCs under MW irradiation. (A) FLIR thermal images of ZIF67@Gr-PEG NC dispersions with different concentrations (0, 1, 2, and 4 mg mL^{-1}) at different time points under MW irradiation. (B) Temperature-raising curves of ZIF67@Gr-PEG NC dispersions under MW irradiation. Statistical analysis (***$P < 0.001$). (C) The corresponding highest temperature increase of ZIF67@Gr-PEG NC dispersions under MW irradiation. (D) DO-BOD test results of the dissolved oxygen concentration of H_2O_2 solutions added with different concentrations of ZIF67@Gr-PEG NCs (0, 1, 2, and 4 mg mL^{-1}) and exposed to MW irradiation for 15 min.

dissolved oxygen was measured using a dissolved oxygen meter after mixing H_2O_2 with different concentrations of ZIF67@Gr-PEG NCs (0, 1, 2, and 4 mg mL^{-1}) and exposing the suspensions to 1.8 W MW irradiation (450 MHz) for 15 min. An increase of MW responsive-dissolved oxygen was observed with the irradiation time (Fig. 2D). Little dissolved oxygen was seen in the pure H_2O_2 group under MW irradiation. By contrast, more dissolved oxygen was produced in H_2O_2 solution containing ZIF67@Gr-PEG NCs. In addition, a substrate concentration-dependent increase in the oxygen concentration was also observed. The oxygen concentration in H_2O_2 solution containing 1, 2, and 4 mg mL^{-1} of ZIF67@Gr-PEG NCs increased by 3.64×10^5, 5.51×10^5 and 6.76×10^5 mol L^{-1} after 15 min irradiation, respectively. The oxygen produced by ZIF67@Gr-PEG NCs in H_2O_2 solution at 1, 2, and 4 mg mL^{-1} was calculated to be 1.47, 2.23 and 2.74 times as high as that of the bare H_2O_2 solution under MW irradiation. The extracellular test results proved that ZIF67@Gr-PEG NCs possessed excellent MW-responsive catalytic ability.

2.4. *In vitro* tumor cell inhibition

Before measuring its killing effects on tumor cells, the *in vitro* cytotoxicity of ZIF67@Gr-PEG NCs was tested using CCK-8 assay. OMECs (human oral mucosal epithelial cells) and SACC-83 cells (human salivary adenoid cystic carcinoma cells) were incubated with ZIF67@Gr-PEG NCs at different concentrations (0, 12.5, 25, 50, 75, 100 and 200 μg mL^{-1}) for 24 h. The ZIF67@Gr-PEG NCs presented an improved biocompatibility after PEG modification (Fig. 3A and B). The cell viability of SACC-83 and HNOECs cells were more than 80% when the ZIF67@Gr-PEG NCs dose reached 100 μg mL^{-1}, revealing low toxicity and favorable biocompatibility of ZIF67@Gr-PEG NCs. Subsequently, we explored the *in vitro* antitumor capability of ZIF67@Gr-PEG NCs under MW irradiation. The SACC-83 cells were incubated with ZIF67@Gr-PEG NCs for 24 h at 100 μg mL^{-1}, and exposed to 1 W, 2450 MHz MW irradiation for 1, 2 and 3 min, respectively. The CCK-8 results showed that, with increasing irradiation time, more cells incubated with ZIF67@Gr-PEG NCs were killed compared with those of the control group incubated without ZIF67@Gr-PEG NCs (Fig. 3C). Only 44.66% of cells taken up by ZIF67@Gr-PEG NCs survived after 3 min MW exposure. Moreover, fluorescence staining (Fig. S1†) and flow cytometry analysis (Fig. 3D and E) of live and dead cells further proved the ability of ZIF67@Gr-PEG NC-induced MW ablation to kill cancer cells, which was in accordance with the results in Fig. 3B.

2.5. Systematic acute toxicity *in vivo*

The systemic toxicity of ZIF67@Gr-PEG NCs was measured by hematological parameters, the body weight, and hematoxylin and eosin (H & E) staining on major organs (Fig. 4). ZIF67@Gr-PEG NCs at different concentrations of 0, 25, 50, 75 and 100 mg

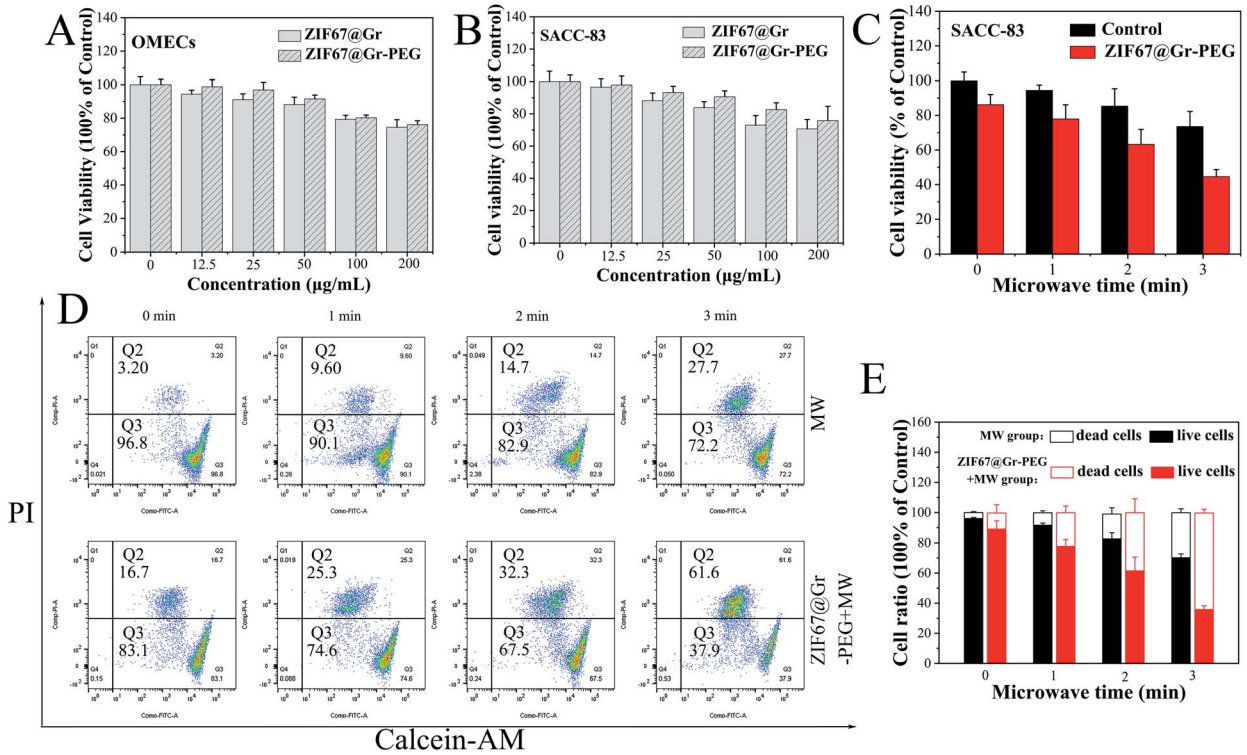

Fig. 3 *In vitro* inhibitory effects of ZIF67@Gr-PEG NCs plus MW irradiation on SACC cells. (A and B) The cytotoxicity of ZIF67@Gr-PEG NCs on OMECs and SACC-83 cells at different concentrations (0, 12.5, 25, 50, 75, 100 and 200 μg mL^{-1}) after incubation for 24 h. (C) Cell viability of SACC-83 cells with or without ZIF67@Gr-PEG NCs exposed to MW irradiation (1 W, 2450 MHz) for 1, 2, and 3 min. (D) Live/dead cell ratio of differently treated groups. Live/dead cells were in the Q3/Q2 region, respectively. (E) Flow cytometric analysis of calcein-AM/PI co-stained SACC-83 cells treated under different conditions.

kg^{-1} were administered into mice by tail intravenous injection. Within the first 24 h after administration, a slight passive behavior and loss of appetite appeared in the mice exposed to 100 mg kg^{-1}, but the mice behaviors returned to normal after 48 h. The body weight showed no obvious abnormal results among the groups during the whole observation period (Fig. S2†). After the mice were sacrificed on day 14, the blood routine and blood biochemical parameters, such as the WBC, RBC, HCT, HGB, MCH, MCV, MPV, PLT, ALT, and CREA in all treated groups, were within normal ranges, but the index of AST and UREA in the group injected with ZIF67@Gr-PEG NCs at 100 mg kg^{-1} was a little higher than that of the control group (Fig. 4A). Moreover, the results of the H&E staining showed that no obvious abnormalities were observed in the heart, spleen, lungs and kidneys at different doses, but chronic pathological toxicity was found in the liver when the administration reached 100 mg kg^{-1} (Fig. 4B and S3†). The above results indicated that the maximum tolerance dose of the ZIF67@Gr-PEG NCs was about 75 mg kg^{-1}, demonstrating good biological safety of ZIF67@Gr-PEG NCs, which can be further used for *in vivo* antitumor studies.

2.6. *In vivo* tumor therapy

Before assessing the synergistic antitumor efficacy of our strategy for MW ablation, we firstly investigated the unfavorable outcomes of insufficient MW ablation and verified the potential of ZIF67@Gr-PEG NCs for addressing the problems of traditional MW ablation. Nude mice bearing SACC tumors were randomly classified into four groups (control, NCs only, MW only, and NCs + MW). When the tumor size reached 200–300 mm^3, the mice were intravenously injected with ZIF67@Gr-PEG NC solution (50 mg kg^{-1}). At 6 h post-injection, the treated mice were anesthetized and treated with 2 W MW irradiation (2450 MHz) for 2 min. The experimental results of the control group and MW alone group in the animal experiment were used to evaluate the therapeutic efficacy of traditional MW ablation. As seen from FLIR images, the MW alone treated group exhibited a characteristic of mild temperature rise (Fig. 5A), which agreed with the fact that traditional MW ablation has the shortcoming of incomplete heat delivery and may lead to insufficient ablation results. Notably, incomplete radiofrequency thermal ablation has been reported to increase the recurrence and metastasis rate of tumors. Next, we will study whether incomplete microwave thermal ablation would also accelerate tumor recurrence and metastasis. As is well known, tumor hypoxia can instigate tumor angiogenesis and correspondingly promote tumor recurrence and metastasis through the activation of HIF-1α and downstream effector genes like VEGF-A.[42] Thus, we continued to investigate the levels of tumor hypoxia and angiogenesis after MW ablation between the control group and MW alone group by measuring the expression levels of HIF-1α,

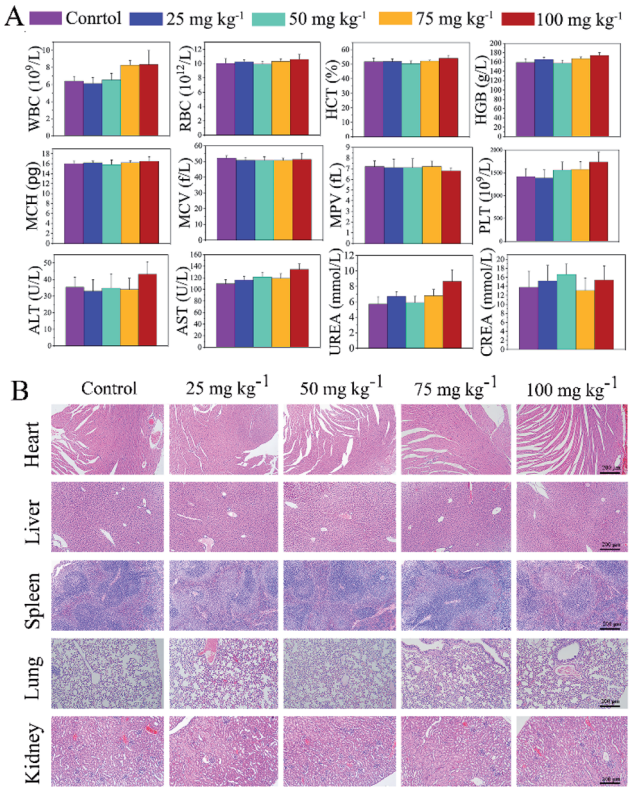

Fig. 4 Acute toxicity test of ZIF67@Gr-PEG NCs. (A) Blood examinations of mice after 14 days of the acute toxicity test. (B) Corresponding H&E staining of major tissues from healthy normal mice after intravenous injection with ZIF67@Gr-PEG NCs for 14 days. The scale bar is 200 μm.

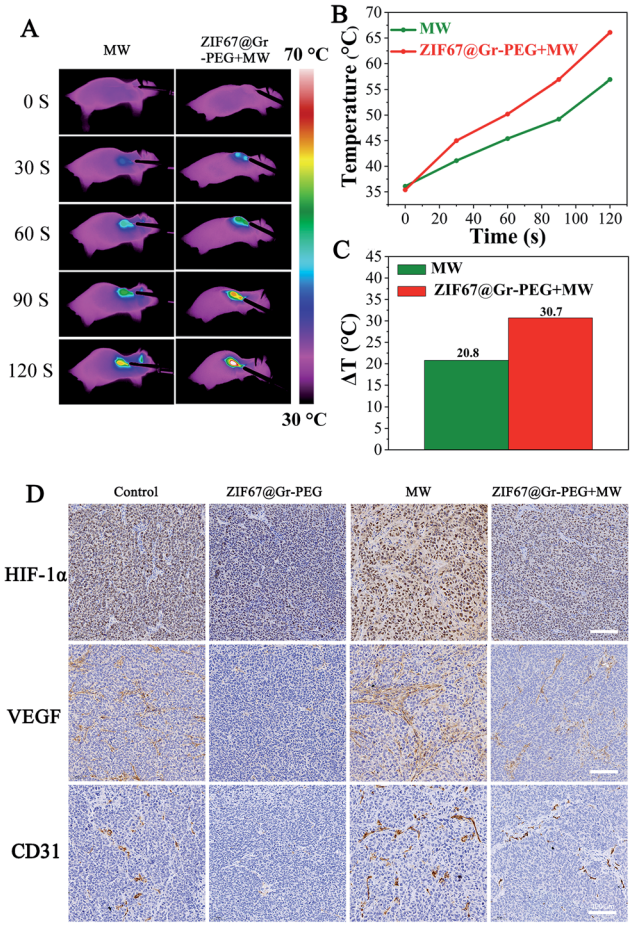

Fig. 5 Heat-generation and hypoxia-ameliorating performances of ZIF67@Gr-PEG NCs in the MW ablation experiment. (A) FLIR images of mice treated with MW ablation alone and ZIF67@Gr-PEG NCs plus MW ablation. (B) Corresponding temperature curves of the mice with different ablation treatments. (C) Comparison of the final temperature changes between the two groups. (D) Immunohistochemical results of HIF-1α, VEGF and CD31 in tumor tissues after different treatments. The scale bar is 100 μm.

VEGF and CD31 using immunohistochemical staining (IHC). The expressions of HIF-1α, VEGF and CD31 in the MW alone group were significantly upregulated compared to those of the control group (Fig. 5D), which implied that insufficient MW ablation treatment aggravated tumor hypoxia and increased tumor angiogenesis, ultimately accelerating tumor progression and recurrence. In an animal experiment, simple MW ablation with a low power of 2 W, 2450 MHz for 2 min could not completely damage tumor cells in the entire region. The hypoxic state worsened by insufficient MW ablation would repurpose these residual tumor cells and instigate tumor angiogenesis. As a result, tumor recurrence was observed on the postoperative day 6 in the mice treated with MW ablation alone. The hypoxia and angiogenesis induced by insufficient MW ablation can be attributed to the following reasons. (1) Tumor vascular damage caused by thermal ablation blocks oxygen supply in tumors, leading to aggravated hypoxia. The level of tumor oxygenation was decreased with the increased damage of blood vessels.[43,44] A high expression of HIFs and prolonged hypoxia were observed after insufficient RFA.[45,46] (2) Activation of tumor-derived endothelial cells and platelets are implicated in cancer metastasis after insufficient thermal ablation, which could directly or indirectly cause angiogenesis and hypoxia.[11,18,19,47,48] J. Kong *et al.* reported that insufficient RFA promoted endothelial permeability and activated platelets in tumors.[18] Besides, activation of platelets could promote the formation of neovascularization as well as thrombosis. Z. Chen observed high expressions of VEGF and CD31 in tumors in the MW alone treated group.[13] (3) Insufficient thermal ablation enhances tumor glycolysis, indicating that tumors are exposed to a sustained hypoxic microenvironment. A previous study found that enhanced HIF-1α stability following insufficient MW ablation led to overexpression of glycolysis-related molecules and promotion of the Warburg effect, which were highly correlated with tumor progression.[12] (4) Insufficient thermal ablation-elicited local inflammation induces angiogenesis and aggravates hypoxia. A recent study reported that after insufficient RFA infiltrating myeloid cells were increased in residual tumors and greater numbers of microvessels were observed in comparation to those in untreated tumors as identified by CD31 staining.[17] Moreover, tumor-associated macrophages could also promote tumor glycolysis and hypoxia.[49] (5) Insufficient thermal ablation disrupts the extracellular matrix to facilitate the formation of

neovascularization.[50,51] Therefore, the traditional MW ablation may suffer unfavorable outcomes of insufficient thermal delivery.

To verify the potential of ZIF67@Gr-PEG NCs for addressing the forementioned problems of traditional MW ablation, we assessed the MW-heating and hypoxia-ameliorating performances of ZIF67@Gr-PEG NCs in MW ablation at the tumor site. The MW heating effects of the tumor surface in mice treated with MW alone and ZIF67@Gr-PEG NCs plus MW were monitored using an infrared thermal imager (Fig. 5A). As depicted in Fig. 5B, in the 2 min period of MW ablation treatment, tumor temperatures of the ZIF67@Gr-PEG NC treated group exhibited rapidly increasing profiles, with a temperature increase of 30.7 °C, from 35.4 °C to 66.1 °C. In contrast, the mice without nanomaterial treatment under MW irradiation showed only a mild temperature increase of 20.8 °C, from 36.1 °C to 56.9 °C. The large increase gap of 9.9 °C between the two groups was attributed to the excellent thermal conversion ability of ZIF67@Gr-PEG NCs in MW ablation (Fig. 5C). The hypoxia-ameliorating effect of ZIF67@Gr-PEG NCs was evaluated by measuring the expression levels of HIF-1α, VEGF and CD31. As shown in Fig. 5D, the expressions of HIF-1α and VEGF were downregulated in ZIF67@Gr-PEG and ZIF67@Gr-PEG + MW groups compared to those of the control group, indicating that ZIF67@Gr-PEG NCs could reestablish normal tumor oxygenation to counteract tumor progression. As expected, the tumor volume in the above two groups was inhibited. By comparing the change of MW ablation with or without ZIF67@Gr-PEG NCs, we found that the expressions of HIF-1α and VEGF in the mice subjected to ZIF67@Gr-PEG NCs plus MW ablation were lower than those in the mice subjected to MW ablation only. These data suggested that ZIF67@Gr-PEG NCs could relieve the insufficient MW ablation-induced hypoxia and block the angiogenic process. Moreover, tumor microvessel density (MVD) quantified based on CD31-positive endothelial cells in tumor tissue assayed by IHC is often used as a potential predictive marker for prognosis. For the tumors singly treated with MW ablation, a notably higher microvessel density compared to the control group was observed, even if their average final volume was actually smaller. By contrast, a significantly lower microvessel density was detected in the tumors treated with ZIF67@Gr-PEG NCs plus MW ablation, with this group showing the highest anti-tumor efficiency among all groups (Fig. 5D). Taken together, owing to the favorable properties of ZIF67@Gr-PEG NCs, our strategy for MW ablation held great potential to achieve good therapeutic effects and prognosis.

The synergistic antitumor efficacy of ZIF67@Gr-PEG NC based MW ablation was evaluated in the above SACC-83 subcutaneous tumor mode. Within 16 days after ablation, the body weight of the mice receiving MW ablation decreased slightly in the first 2 days, and then resumed to increase gradually, while the other two groups exhibited no abnormal changes (Fig. 6A). The tumor volume was monitored every 2 days to assess the therapeutic effects of mice receiving various treatments. The tumors displayed similar growth rates in the control and ZIF67@Gr-PEG NCs groups (Fig. 6B). However, the tumor growth rates in both the ZIF67@Gr-PEG NCs + MW group and the MW alone group were significantly lower than that of the control group, with the

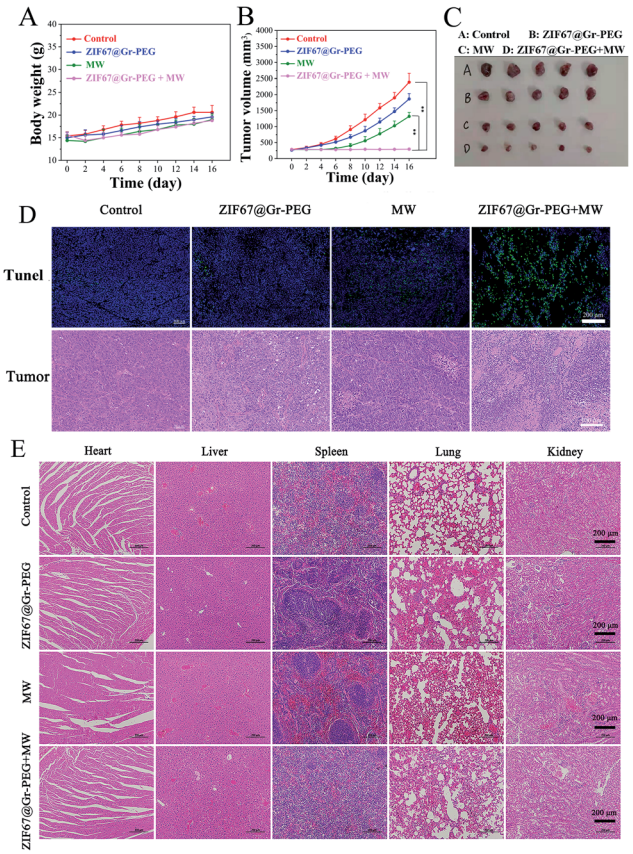

Fig. 6 *In vivo* synergistic anti-tumor effects of ZIF67@Gr-PEG NCs plus MW ablation against SACC tumors. (A) Body weight curves and (B) time-dependent tumor growth after different treatments in SACC tumor bearing mice. *p < 0.05 and **p < 0.01. (C) Tumor tissue pictures. (D) TUNEL staining (the scale bar is 200 μm) and H & E staining (the scale bar is 100 μm) for pathological changes in tumor tissues from different groups. (E) H&E staining of major organs dissected from the treated mice. The scale bar is 200 μm.

former decreasing at a greater level than the latter. The significant tumor volume reduction in the ZIF67@Gr-PEG plus MW group was due to the combined hypoxia-ameliorating and MW-heating effects of ZIF67@Gr-PEG. Then, the treated mice were sacrificed on day 17. The tumor photos were consistent with the above experimental results (Fig. 6C). A high tumor ablation rate could be achieved in the ZIF67@Gr-PEG plus MW group. We also examined tumor apoptosis by H&E staining and TUNEL assay (Fig. 6D). The results showed that ZIF67@Gr-PEG NC based MW ablation effectively triggered tumor apoptosis and coagulative necrosis, while MW alone treatment induced an insufficient ablation effect. These results confirmed that the tumor-located ZIF67@Gr-PEG NCs did have high antitumor efficacy *via* the combination of efficient hyperthermia and *in situ* oxygen production.

3. Experimental section

3.1. Preparation of ZIF67@Gr NCs

Firstly, 2 mg graphene powder was dispersed in 5 mL anhydrous ethanol, and 10 mg PVP was dispersed in 1 mL anhydrous

ethanol. PVP solution was added dropwise to the Gr solution under magnetic stirring at 50 °C and was continuously stirred for 6 h to obtain PVP coated Gr NCs. Next, 25 mg of Co $(NO_3)_2 \cdot 6H_2O$ was dissolved in 4 mL of anhydrous ethanol and 300 mg of 2-methylimidazole (2-MIM) was dissolved in 9 mL of anhydrous ethanol. The Co $(NO_3)_2 \cdot 6H_2O$ and 2-MIM solutions were mixed using a magnetic stirrer under ambient conditions for 2 min, and then PVP coated Gr NCs and 2 mL of PVP solution (20 mg mL^{-1}) were added into the above mixture and continuously stirred for 6 h. The ZIF67@Gr NCs were obtained by centrifugation at 12 000 rpm for 5 min and washed with anhydrous ethanol three times.

3.2. Preparation of ZIF67@Gr-PEG NCs

PEG modification was applied to improve the biocompatibility of ZIF67@Gr NCs. The obtained ZIF67@Gr NCs were added into a 50 mL Erlenmeyer flask filled with 5 mg of mPEG-NH_2 and 10 mL of Tris–HCl under magnetic stirring for 4 h. ZIF67@Gr-PEG NCs were collected by centrifugation and washed with ethanol. Finally, the ZIF67@Gr-PEG NCs were stored at 4 °C.

3.3. Microwave heating experiment *in vitro*

Different amounts of ZIF67@Gr-PEG NCs (0, 1, 2 and 4 mg) were dispersed in 1 mL saline solution and then irradiated with 0.9 W MW power (450 MHz) for 5 min. An FLIR thermal imager was used for real-time temperature monitoring and the temperature value was recorded every 10 s.

3.4. Determination of dissolved oxygen *in vitro*

The experiment was divided into four groups: the $dH_2O + H_2O_2$ + MW group, and three ZIF67@Gr-PEG NCs + H_2O_2 + MW groups, in which the concentrations of ZIF67@Gr-PEG NCs were 1.0, 2.0 and 4.0 mg mL^{-1}, respectively. Then 20 μL of 5% H_2O_2 was added to the solution of ZIF67@Gr-PEG NCs and irradiated at 1.8 W, 450 Hz for 15 min. A DO-BOD detector (dissolved oxygen-biochemical oxygen demand detector) was used for real-time monitoring of dissolved oxygen generated from ZIF67@Gr-PEG NCs under MW irradiation.

3.5. Cytotoxicity assays

The cytotoxicities of ZIF67@Gr-PEG NCs and ZIF67@Gr NCs were evaluated by CCK-8 assay. Human oral mucosal epithelial cells (OMECs) and human salivary adenoid cystic carcinoma cells (SACC-83) with a concentration of 1×10^4 were plated in 96-well plates and cultured under suitable conditions for 24 h (37 °C, 5% CO_2). Different concentrations (0, 12.5, 25, 50, 100 and 200 μg mL^{-1}) of ZIF67@Gr-PEG NCs and ZIF67@Gr NCs were further incubated with cells for 24 h respectively, with each group containing 8 parallels. Next, 10 μL CCK-8 solution (10% CCK-8) was added to each well and the cells were incubated for another 24 h. The absorbance of each well in a 96-well plate was detected using an enzyme labeling apparatus (absorption peak at 450). The cell viability was calculated as follows: cell viability (%) = $(OD_{sample} - OD_{blank})/(OD_{control} - OD_{blank}) \times 100\%$, where $OD_{control}$ represents the absorbance of untreated cells and OD_{blank} represents the culture media without samples or cells.

3.6. *In vitro* tumor cell inhibition

The experiment was divided into four groups: the (1) control group, (2) MW alone group, (3) ZIF67@Gr-PEG NCs alone group and (4) ZIF67@Gr-PEG NCs plus MW group ($n = 8$). 1×10^5 SACC-83 cells were seeded in six-well plates and incubated at 37 °C with 5% CO_2 for 24 h. The culture medium was then replaced with RPMI-1640 (the control group and MW alone group) or with RPMI-1640 containing ZIF67@Gr-PEG NCs at a concentration of 100 μg mL^{-1} (the other two groups). After 24 h of incubation, cells from each group were digested with trypsin/EDTA (0.25%/0.02%, the mass ratio) and redispersed in a complete culture medium for use. Cell suspensions of the MW and ZIF67@Gr-PEG NCs plus MW groups were irradiated after being dispersed in a microwave-heated EP tube at a MW output power of 1 W at 2450 MHz for 1, 2, and 3 min, respectively. Meanwhile, cell suspensions of the control and ZIF67@Gr-PEG NCs alone groups were placed in an EP tube. After MW irradiation, the cells were transplanted to 96-well plates and incubated at 37 °C with 5% CO_2 for 24 h to measure cell viability by CCK-8 assay.

3.7. Live/dead cell viability assay

Live/dead cell staining was also used to evaluate the inhibitory effect of ZIF67@Gr-PEG NCs with different times (0, 1, 2, and 3 min) at the same MW irradiation power (1.0 W). The experimental process was in accordance with the above MW treatment experiment. All cells in the group were collected and stained with calcein-AM and propidium iodide for 30 min at 37.0 °C, and then observed using a fluorescence microscope. The living/dead cell ratio was analyzed by flow cytometry.

3.8. Acute toxicity test

To evaluate the biocompatibility of ZIF67@Gr-PEG NCs *in vivo*, acute toxicity experiments were performed on healthy mice. Different concentrations of ZIF67@Gr-PEG NCs dispersed in 5% glucose solution at 0, 25, 50, 75 and 100 mg kg^{-1} were injected into 25 ICR male mice with a body weight of 20–25 g ($n = 5$) by tail intravenous injection. The growth condition and the body weight of each mouse were monitored daily for 14 days. During the 24 hour physique monitoring of mice, a slight passive behavior accompanied by a loss of appetite appeared in the mice at the dose of 100 mg kg^{-1}, but adverse reactions decreased or disappeared after 48 h. No significant abnormal behaviors were observed in the mice exposed to other doses during the whole experiment. The mice were sacrificed two weeks later. Blood from the angular vein of the eye was collected for blood routine and blood biochemistry tests. Tissue samples from the heart, liver, spleen, lungs, and kidneys were fixed in 10% neutral buffered formalin and embedded in paraffin for the subsequent histological study.

3.9. *In vivo* antitumor efficacy

BALB/c Nude mice bearing SACC-83 tumor cells were used to explore the antitumor efficacy of ZIF67@Gr-PEG NCs, in compliance with the requirements of the Institutional Animal Care Committee. Female BALB/c nude mice were employed as experimental mice. The tumor model was set up by subcutaneous injection of 100 μL SACC-83 tumor cells (2×10^7) into the right armpit of nude mice. When the tumor volumes reached 200–300 mm^3, the mice were randomly divided into four groups: the (1) control group, (2) ZIF67@Gr-PEG NCs alone group, (3) MW alone group and (4) ZIF67@Gr-PEG NCs plus MW group. ZIF67@Gr-PEG NCs dispersed in 5% glucose solution were injected through the tail vein at 50 mg kg^{-1} in the ZIF67@Gr-PEG NCs and ZIF67@Gr-PEG NCs plus MW groups. Meanwhile, an equivalent volume of 5% glucose solution was given to the mice in the control and MW groups. Six hours after injection, the mice in the MW and ZIF67@Gr-PEG NCs plus MW groups underwent MW irradiation at 2 W (2450 MHz, continuous wave). During the MW treatment, an FLIR system was applied to monitor temperature changes and record thermal imaging results. The tumor volume and body weight were recorded every two days during the whole process. The tumor volume was calculated according to the following formula: tumor volume (mm^3) = (length × $width^2$)/2. On day 17, the tumors and major organs were excised and fixed with 10% neutral buffered formalin. Thereafter, issue sections were used for H & E staining, IHC staining and TUNEL assay. Mice were euthanized according to the standard animal welfare guidelines.

3.10. Statistical analysis

The results were expressed as the mean ± SD. The statistical analysis was performed using SPSS 26.0 software (SPSS, Inc., Chicago, IL, USA). All data were analyzed using the one-way ANOVA analysis. Statistical significance was denoted by $*p < 0.05$, $**p < 0.01$, and $***p < 0.001$.

4. Conclusions

In summary, for the first time, nanomaterial-based MW ablation was applied in head and neck tumors. We have developed a novel MW responsive ZIF67/graphene composite for improved MW ablation. Graphene served as a MW sensitizer for high-performance MW ablation and ZIF67 was employed as an oxygen self-sufficient nanoagent for tumor hypoxia relief. In contrast to traditional MW ablation that is deficient in heat delivery and tends to cause a deteriorated hypoxic environment, our strategy for MW ablation is able to improve MW ablation efficiency, normalize the hypoxic TME and activate innate antitumor immune responses. These advantages are thought to be important for the long-term inhibition of tumors with a high rate of recurrence and metastasis. More importantly, the improved strategy not only promotes the translation of thermotherapeutic graphene from basic research to clinical practice but also diversifies the application of MW ablation to more areas.

There is still ample room for further investigating the functions of ZIF67@Gr based-nanocomposites for MW ablation therapy. As the cells we used were derived from humans, in this work we only explored the hypoxia-ameliorating and MW thermal effects of ZIF67@Gr-PEG NC induced MW ablation by transplanting SACC cells into the immune-deficient nude mice. In future research, we will investigate the systemic immune response of our strategy by coupling with PD-L1/PD-1 immunotherapy in mice with a reconstituted human immune system. Moreover, surface modification, either through affecting catalytic activity or by affecting the biodistribution and intracellular fate, plays an important role in governing the antitumor activity of nanoparticles.[37] We could also utilize some surface modification strategies to improve the antitumor performances of ZIF67@Gr based-nanocomposites, such as targeting tumor-associated immune cells, improving the precision of subcellular localization, *etc.*

Author contributions

Conceptualzation: Ning Wen and Yaping Tian. Methodology: Ruozhen Li. Investigation: Ruozhen Li, Yu Wang, Ruijie Dang, Lisheng Zhao, Yun Xia Li, Suo Yang and Biao Zhu. Statistical data analysis: Ruozhen Li. Writing – original and draft: Ruozhen Li. Writing – review & editing: Ning Wen. Supervision: N. Wen.

Conflicts of interest

The authors declare that they have no known competing financial interests or personal relationships that could have appeared to influence the work reported in this paper.

Acknowledgements

The authors declare no competing financial interest.

Notes and references

1 Y. Drier, M. J. Cotton, K. E. Williamson, S. M. Gillespie, R. J. H. Ryan and M. J. Kluk, *Nat. Genet.*, 2016, **48**, 265–272.
2 J. Fordice, C. Kershaw, A. El-Naggar and H. Goepfert, *Arch. Otolaryngol., Head Neck Surg.*, 1999, **125**, 149–152.
3 A. D. Rapidis, N. Givalos, H. Gakiopoulou, G. Faratzis, S. D. Stavrianos, G. A. Vilos, E. E. Douzinas and E. Patsouris, *Oral Oncol.*, 2005, **41**, 328–335.
4 S. Jang, P. N. Patel, R. J. Kimple and T. M. McCulloch, *Anticancer Res.*, 2017, **37**, 3045–3052.
5 W. Dai, Y. Yao, Q. Zhou and C. F. Sun, *PLoS One*, 2014, **23**, e87148.
6 R. L. Dodd and N. J. Slevin, *Oral Oncol.*, 2006, **42**, 759–769.
7 W. Wang, J. Ma, F. Jin and J. Liao, *Exp. Ther. Med.*, 2017, **14**, 3105–3111.
8 D. Long, J. Mao, T. Liu, C. Fu, L. Tan, X. Ren, H. Shi, H. Su, J. Ren and X. Meng, *Nanoscale*, 2016, **8**, 11044–11051.
9 J. P. Dou, Q. Wu, C. H. Fu, D. Y. Zhang, J. Yu, X. W. Meng and P. Liang, *J. Nanobiotechnol.*, 2019, **17**, 118.

10 Y. Cao, Y. Zhou, J. Pan, X. Zhong, J. Ding, X. Jing and S. Sun, *Chem. Eng. J.*, 2021, **422**, 130111.
11 P. Kong, H. Pan, M. Yu, L. Chen, H. Ge, J. Zhu, G. Ma, L. Li, Q. Ding, W. Zhou and S. Wang, *Oncotarget*, 2017, **8**, 115089–115101.
12 Y. Chen, J. Bei, M. Liu, J. Huang, L. Xie, W. Huang, M. Cai, Y. Guo, L. Lin and K. Zhu, *Cancer Lett.*, 2021, **518**, 23–34.
13 Z. Chen, Q. Wu, W. Guo, M. Niu, L. Tan, N. Wen, L. Zhao, C. Fu, J. Yu, X. Ren, P. Liang and X. Meng, *Biomaterials*, 2021, **276**, 121016.
14 M. Moussa, S. N. Goldberg, G. Kumar, R. R. Sawant, T. Levchenko, V. Torchilin and M. Ahmed, *J. Vasc. Intervent. Radiol.*, 2014, **25**, 1972–1982.
15 S. G. Kroeze, H. H. van Melick, M. W. Nijkamp, F. K. Kruse, L. W. Kruijssen, P. J. van Diest, J. L. Bosch and J. J. Jans, *BJU Int.*, 2012, **110**, E281–E286.
16 A. L. Halpern, J. G. Fitz, Y. Fujiwara, J. Yi, A. L. Anderson, Y. Zhu, R. D. Schulick, K. C. El Kasmi and C. C. Barnett, *Am. J. Physiol.: Cell Physiol.*, 2021, **320**, 142–151.
17 L. Shi, J. Wang, N. Ding, Y. Zhang, Y. Zhu, S. Dong, X. Wang, C. Peng, C. Zhou, L. Zhou, X. Li, H. Shi, W. Wu, X. Long, C. Wu and W. Liao, *Nat. Commun.*, 2019, **10**, 5421.
18 J. Kong, C. Yao, S. Dong, S. Wu, Y. Xu, K. Li, L. Ji, Q. Shen, Q. Zhang, R. Zhan, H. Cui, C. Zhou, H. Niu, G. Li, W. Sun and L. Zheng, *Adv. Sci.*, 2021, **8**, 2002228.
19 S. Iwahashi, M. Shimada, T. Utsunomiya, S. Imura, Y. Morine, T. Ikemoto, C. Takasu, Y. Saito and S. Yamada, *Cancer Lett.*, 2016, **375**, 47–50.
20 J. C. Nault, O. Sutter, P. Nahon, N. Ganne-Carrié and O. Séror, *J. Hepatol.*, 2018, **68**, 783–797.
21 Z. Chen, W. Guo, Q. Wu, L. Tan, T. Ma, C. Fu, J. Yu, X. Ren, J. Wang, P. Liang and X. Meng, *Theranostics*, 2020, **10**, 4659–4675.
22 Z. Chen, M. Niu, G. Chen, Q. Wu, L. Tan, C. Fu, X. Ren, H. Zhong, K. Xu and X. Meng, *ACS Nano*, 2018, **12**, 12721–12732.
23 Q. Du, T. Ma, C. Fu, T. Liu, Z. Huang, J. Ren, H. Shao, K. Xu, F. Tang and X. Meng, *ACS Appl. Mater. Interfaces*, 2015, **7**, 13612–13619.
24 T. Li, Q. Wu, W. Wang, Z. Chen, L. Tan, J. Yu, C. Fu, X. Ren, P. Liang, J. Ren, L. Ma and X. Meng, *Biomaterials*, 2020, **234**, 119773.
25 H. Shi, T. Liu, C. Fu, L. Li, L. Tan, J. Wang, X. Ren, J. Ren, J. Wang and X. Meng, *Biomaterials*, 2015, **44**, 91–102.
26 S. Wang, L. Tan, P. Liang, T. Liu, J. Wang, C. Fu, J. Yu, J. Dou, H. Li and X. Meng, *J. Mater. Chem. B*, 2016, **4**, 2133–2141.
27 C. Fu, F. He, L. Tan, X. Ren, W. Zhang, T. Liu, J. Wang, J. Ren, X. Chen and X. Meng, *Nanoscale*, 2017, **9**, 14846–14853.
28 C. Fu, H. Zhou, L. Tan, Z. Huang, Q. Wu, X. Ren, J. Ren and X. Meng, *ACS Nano*, 2018, **12**, 2201–2210.
29 Q. Wu, N. Xia, D. Long, L. Tan, W. Rao, J. Yu, C. Fu, X. Ren, H. Li, L. Gou, P. Liang, J. Ren, L. Li and X. Meng, *Nano Lett.*, 2019, **19**, 5277–5286.
30 H. Shi, M. Niu, L. Tan, T. Liu, H. Shao, C. Fu, X. Ren, T. Ma, J. Ren, L. Li, H. Liu, K. Xu, J. Wang, F. Tang and X. Meng, *Chem. Sci.*, 2015, **6**, 5016–5026.
31 Y. Sun, Z. Chen, H. Gong, X. Li, Z. Gao, S. Xu, X. Han, B. Han, X. Meng and J. Zhang, *Adv. Mater.*, 2020, **32**, e2002024.
32 Y. Sun, L. Yang, K. Xia, H. Liu, D. Han, Y. Zhang and J. Zhang, *Adv. Mater.*, 2018, **21**, e1803189.
33 J. Li, K. Wei, S. Zuo, Y. Xu, Z. Zha, W. Ke, H. Chen and Z. Ge, *Adv. Funct. Mater.*, 2017, **27**, 1702108.
34 G. Song, C. Liang, X. Yi, Q. Zhao, L. Cheng, K. Yang and Z. Liu, *Adv. Mater.*, 2016, **28**, 2716–2723.
35 R. Liang, L. Liu, H. He, Z. Chen, Z. Han, Z. Luo, Z. Wu, M. Zheng, Y. Ma and L. Cai, *Biomaterials*, 2018, **177**, 149–160.
36 S. Z. Ren, B. Wang, X. H. Zhu, D. Zhu, M. Liu, S. K. Li, Y. S. Yang, Z. C. Wang and H. L. Zhu, *ACS Appl. Mater. Interfaces*, 2020, **12**, 24662–24674.
37 G. Tang, J. He, J. Liu, X. Yan and K. Fan, *Exploration*, 2021, **1**, 75–89.
38 R. Slovak, J. M. Ludwig, S. N. Gettinger, R. S. Herbst and H. S. Kim, *Journal for ImmunoTherapy of Cancer*, 2017, **5**, 78.
39 T. Zhou, X. Liang, P. Wang, Y. Hu, Y. Qi, Y. Jin, Y. Du, C. Fang and J. Tian, *ACS Nano*, 2020, **14**, 12679–12696.
40 J. Z. Du, H. J. Li and J. Wang, *Acc. Chem. Res.*, 2018, **51**, 2848–2856.
41 Y. Dai, C. Xu, X. Sun and X. Chen, *Chem. Soc. Rev.*, 2017, **46**, 3830–3852.
42 R. Abou Khouzam, K. Brodaczewska, A. Filipiak, N. A. Zeinelabdin, S. Buart, C. Szczylik, C. Kieda and S. Chouaib, *Front. Immunol.*, 2021, **11**, 613114.
43 L. Feng, L. Cheng, Z. Dong, D. Tao, T. E. Barnhart, W. Cai, M. Chen and Z. Liu, *ACS Nano*, 2017, **11**, 927–937.
44 K. Haedicke, L. Agemy, M. Omar, A. Berezhnoi, S. Roberts, C. Longo-Machado, M. Skubal, K. Nagar, H. T. Hsu, K. Kim, T. Reiner, J. Coleman, V. Ntziachristos, A. Scherz and J. Grimm, *Nat. Biomed. Eng.*, 2020, **4**, 286–297.
45 M. W. Nijkamp, J. D. van der Bilt, M. T. de Bruijn, I. Q. Molenaar, E. E. Voest, P. J. van Diest, O. Kranenburg and I. H. Borel Rinkes, *Ann. Surg.*, 2009, **249**, 814–823.
46 Y. Tong, H. Yang, X. Xu, J. Ruan, M. Liang, J. Wu and B. Luo, *Cancer Sci.*, 2017, **108**, 753–762.
47 J. Kong, L. Kong, J. Kong, S. Ke, J. Gao, X. Ding, L. Zheng, H. Sun and W. Sun, *J. Transl. Med.*, 2012, **10**, 230.
48 S. Yoshida, M. Kornek, N. Ikenaga, M. Schmelzle, R. Masuzaki, E. Csizmadia, Y. Wu, S. C. Robson and D. Schuppan, *Hepatology*, 2013, **58**, 1667–1680.
49 H. Jeong, S. Kim, B. J. Hong, C. J. Lee, Y. E. Kim, S. Bok, *et al.*, *Cancer Res.*, 2019, **79**, 795–806.
50 V. Raeesi and W. C. Chan, *Nanoscale*, 2016, **8**, 12524–12530.
51 J. Kolosnjaj-Tabi, I. Marangon, A. Nicolas-Boluda, A. K. A. Silva and F. Gazeau, *Pharmacol. Res.*, 2017, **126**, 123–137.